Liviu Movileanu[†]
James M. Benevides
George J. Thomas Jr.
Division of Cell Biology and Biophysics, School of Biological Sciences, University of Missouri—Kansas City, Kansas City, MO 64110

Temperature Dependence of the Raman Spectrum of DNA. II. Raman Signatures of Premelting and Melting Transitions of Poly(dA)·Poly(dT) and Comparison with Poly(dA-dT)·Poly(dA-dT)*

Abstract: *The temperature dependence of the Raman spectrum of poly(dA)·poly(dT) (dA: deoxyadenosine; dT: thymidine), a model for DNA containing consecutive adenine·thymine (A·T) pairs, has been analyzed using a spectrometer of high spectral precision and sensitivity. Three temperature intervals are distinguished: (a) premelting (10 < t < 70°C), in which the native double helix is structurally altered but not dissociated into single strands; (b) melting (70 < t < 80°C), in which the duplex is dissociated into single strands; and (c) postmelting (80 < t°C), in which no significant structural change can be detected. The distinctive Raman difference signatures observed between 10 and 70°C and between 70 and 80°C are interpreted in terms of the structural changes specific to premelting and melting transitions, respectively. Premelting alters the low-temperature conformation of the deoxyribose-phosphate backbone and eliminates base hydrogen bonding that is distinct from canonical Watson–Crick hydrogen bonding; these premelting perturbations occur without disruption of base stacking. Conversely, melting eliminates canonical Watson–Crick pairing and base stacking. The results are compared with those reported previously on poly(dA-dT)·poly(dA-dT), the DNA structure consisting of alternating A·T and T·A pairs (L. Movileanu, J. M. Benevides, and G. J. Thomas, Jr. Journal of Raman Spectroscopy, 1999, Vol. 30, pp. 637–649). Poly(dA)·poly(dT) and poly(dA-dT)·poly(dA-dT) exhibit strikingly dissimilar temperature-dependent Raman profiles prior to the onset of melting. However, the two duplexes exhibit very similar melting transitions, including the same Raman indicators of ruptured Watson–Crick pairing, base unstacking and collapse of backbone order. A detailed analysis of the data provides a comprehensive Raman assignment scheme for adenosine and thymidine residues of B-DNA, delineates Raman markers diagnostic of consecutive A·T and alternating A·T/T·A tracts of DNA, and identifies the distinct Raman difference signatures for premelting and melting transitions in the two types of sequences.* © 2002 John Wiley & Sons, Inc. Biopolymers 63: 181–194, 2002; DOI 10.1002/bip.10022

Keywords: *B-DNA; premelting; adenine·thymine pair; hydrogen bond; vibrational assignments*

INTRODUCTION

Double-stranded (ds) DNA containing only adenine·thymine (A·T) base pairs exhibits physical characteristics not observed for other members of the B-DNA family of secondary structures.[1–4] Among these is the property of premelting, i.e., temperature-dependent structural polymorphism below the temperature (T_m) at which dissociation into single strands occurs. Although CD spectra suggest that such premelting is common to many AT-rich DNA sequences,[5] evidence has been presented that premelting may be specific to dsDNA containing repeats of adenine (A-tract) and thymine (T-tract) along complementary strands.[6–8] The biological significance of the A-tract derives from its occurrence in native kinetoplast DNA.[6] The A-tract may also play a role in the anomalous gel mobilities observed for oligo(dA)·oligo(dT) (dA: deoxyadenosine; dT: thymidine) and kinetoplast DNA sequences.[1,2,6,9,10] Such electrophoretic behavior has been attributed to the induction or stabilization of DNA curvature. Because increases of temperature that promote premelting also mitigate anomalous gel mobility, it has been proposed that both effects reflect a low-temperature structure specific to the A-tract.[2,4,10] However, the defining features of such an A-tract conformation and the detailed structural changes that may take place during premelting remain largely unresolved. Whether premelting is specific to DNA containing oligo(dA)·oligo(dT) tracts or inclusive of alternating A·T/T·A tracts also remains an open question.[11]

The temperature dependence (10 < t < 90°C) of the Raman spectrum of poly(dA-dT)·poly(dA-dT), the double-helical B-DNA containing A·T and T·A pairs in alternating sequence, was recently analyzed in detail.[12] The results demonstrate that poly(dA-dT)·poly(dA-dT), despite the absence of A-tracts, undergoes a premelting phase (10 < t < 66°C) prior to the onset of the canonical melting transition (66 < t < 75°C). The majority of Raman bands in the spectrum of poly(dA-dT)·poly(dA-dT) are affected greatly by both the premelting and melting transitions. Unique Raman signatures of premelting and melting have been identified. The previous analysis has also revealed several novel Raman bands diagnostic of A·T pairing and stacking in poly(dA-dT)·poly(dA-dT).[12] Of particular interest is a Raman band of the thymidine moiety occurring at 1182 cm^{-1}. The 1182 cm^{-1} band, which had not been recognized previously as a sensitive marker of DNA secondary structure, exhibits maximum intensity when the dT residue is unpaired, as in poly(dT) or thermally denatured poly(dA-dT). Conversely, the intensity of the 1182 cm^{-1} band diminishes proportionally to zero when unpaired dT becomes paired with dA, as in B-DNA. Structural characterization of the 1182 cm^{-1} marker was facilitated by the use of a recently designed Raman spectrophotometer of high sensitivity, which permits accurate quantitative measurement of temperature-dependent Raman band intensities and frequencies.

Here, we analyze in detail the temperature dependence of the Raman signature of poly(dA)·poly(dT), a model for B-DNA containing the A-tract. Although vibrational spectra of poly(dA)·poly(dT) have been reported previously,[13–15] the temperature dependence has not been probed in detail. The present results are interpreted in connection with the recent findings on premelting and melting in poly(dA-dT)·poly(dA-dT)[12] and previously reported Raman, infrared and ab initio results on related model structures.[13,14,16–27] We demonstrate that the low temperature structures of poly(dA)·poly(dT) and poly(dA-dT)·poly(dA-dT) are distinguished by characteristic Raman signatures and that these distinguishing features are sustained throughout the premelting phase. Interestingly, dA and dT residues as well as the sugar-phosphate backbones of poly(dA)·poly(dT) and poly(dA-dT)·poly(dA-dT) exhibit Raman markers differing from those of genomic B-DNA of mixed base composition.

The emphasis in the present study is on determining how the vibrational bands of poly(dA)·poly(dT) change with temperature. The results are used to develop an understanding of the structural significance of temperature-dependent Raman bands of DNA containing A-tracts. In combination with previous results on poly(dA-dT)·poly(dA-dT),[12] the findings also provide an improved basis for interpretation of the temperature-dependent vibrational spectrum of genomic DNA of mixed base sequence. In a related study, we show that the temperature-dependent Raman properties of poly(dA)·poly(dT) and poly(dA-dT)·poly(dA-dT) can also be exploited to evaluate thermodynamic parameters of premelting and melting transitions in the two structures (L. Movileanu, J. M. Benevides, and G. J. Thomas, Jr., in preparation).

MATERIALS AND METHODS

Sample Preparation

Poly(dA)·poly(dT) was obtained as the sodium salt from Amersham Pharmacia Biotech (Alameda, CA). Sedimentation analysis indicated a sedimentation velocity coefficient ($S_{20,w}$) of 19.9 Svedberg, corresponding to an average mo-

lecular weight of 6400 kDa [~9700 base pairs (bp)]. The high molecular weight of the duplex diminishes end effects, which is favorable to thermodynamic analysis of the data, to be reported elsewhere (L. Movileanu, J. M. Benevides, and G. J. Thomas, Jr., in preparation). Samples were dissolved to 30–40 mg/mL in H_2O containing 100 mM NaCl at pH 7.0 ± 0.1. Aliquots (~6 μL) of the solutions were degassed, sealed in glass capillaries (Kimax no. 34502) and thermostated at the indicated temperatures during data collection.[28]

Raman Spectroscopy

Raman spectra were excited with the 514.5 nm argon line of a Coherent Innova laser and collected on a single spectrograph (Spex model 500M; ISA Edison NJ, USA) described previously.[12] The radiant power at the sample was ~200 mW. Typically 7–12 accumulations of 10 s each were averaged to generate the spectra presented below. Noteworthy features of this instrumentation are a holographic bandpass filter to eliminate interfering laser emissions, a notch filter to reject Rayleigh scattering, and a liquid-nitrogen cooled charge-coupled device to provide state-of-the-art quantum efficiency in Raman photon detection. In terms of overall signal-to-noise ratio, the presently obtained Raman spectra of poly(dA)·poly(dT) are between one and two orders of magnitude improved over previously published results.[13,27] Additional performance features of the spectrometer design have been discussed by Carey and coworkers in applications to proteins.[29] Raman frequencies (wavenumber values) are accurate to within ±0.5 cm^{-1}.

Raman spectra were collected at approximately 5°C intervals in the range 5–95°C on samples maintained to within ±0.5°C of the indicated temperature. Raman intensities were normalized using the peak height of the band at 1092 cm^{-1}, which is assigned to the PO_2^- symmetric stretching mode of the polydeoxynucleotide phosphate groups. The peak height of the 1092 cm^{-1} band has been demonstrated as a reliable intensity standard for both polydeoxynucleotides and genomic DNA of the B conformation throughout the temperature range 10–90°C.[20,30] The reliability of the 1092 cm^{-1} band was verified independently in the present study (data not shown) using the 980 cm^{-1} band of SO_4^{2-} (Na_2SO_4, added as an intensity standard).[20] Presentation of digital difference spectra is used as in previous work to identify specific Raman band intensity changes or wavenumber shifts as a function of temperature.[12,20,22,31]

RESULTS AND INTERPRETATION

Temperature Dependence of the Raman Spectrum of Poly(dA)·Poly(dT)

Poly(dA)·poly(dT) forms a double helix in the B-DNA family of secondary structures, as indicated by fiber x-ray diffraction[32,33] and solution Raman spectroscopy.[27,33,37] X-ray crystallography of the A-tract model, d(CGCAAAAAAGCG)·d(CGCTTTTTTGCG), also confirms a B-like conformation in the central oligo(dA)·oligo(dT) segment, although with the unusual feature of bifurcated hydrogen bonds.[3] Additional nonstandard features of poly(dA)·poly(dT) are a narrow minor groove,[32] a high degree of hydration,[36] and a propensity toward polymorphism, promoted by changes in temperature, relative humidity, or chemical environment.[2,33,37] Here, we investigate the temperature dependence of the Raman spectrum of poly(dA)·poly(dT) in physiological salt solution (100 mM NaCl). The results are compared with a corresponding study of poly(dA-dT)·poly(dA-dT).[12]

Raman spectra (600–1800 cm^{-1}) of double-helical poly(dA)·poly(dT) (10°C) and of fully denatured poly(dA) and poly(dT) single strands (85°C) are shown in the bottom and top traces, respectively, of the left panel of Figure 1. Other traces of this panel show difference spectra computed at intervals of approximately 5°C between the indicated intermediate temperature (minuend) and 10°C (subtrahend). These difference spectra illustrate that although the most pronounced spectral changes occur between 70 and 80°C, the Raman signature of poly(dA)·poly(dT) is sensitive to temperature throughout the range $10 < t < 80$°C. In the interval 10–70°C, the spectral changes consist primarily of shifts in Raman band frequencies, typical of highly localized structural perturbations; conversely, in the interval 70–80°C large increases are also observed in the intensities of many Raman bands, indicating recovery of Raman hypochromism. The latter interval defines the cooperative *melting* transition of poly(dA)·poly(dT), and the observed spectral intensity changes reflect both unstacking and unpairing of bases attendant with strand separation. Raman bands diagnostic of melting are those near 727 and 1182 cm^{-1}, as illustrated in Figure 2. Quantitative measurement of the Raman intensity increase at 1182 cm^{-1} with temperature indicates a median melting temperature (T_m) of 76.5 ± 0.4°C for the cooperative transition. The spectral changes observed prior to the onset of melting represent the *premelting* transition of poly(dA)·poly(dT). Premelting is noncooperative, as exemplified by the temperature-dependent profiles of bands near 842 and 1513 cm^{-1} shown in Figures 3 and 4, respectively. In accordance with previous determinations,[12,20] the phosphodioxy (PO_2^-) marker band at 1092 cm^{-1} exhibits neither a significant wavenumber shift nor an appreciable intensity change with temperature, and serves as the primary basis for normalization of intensity and wavenumber values of other Raman bands in the spectrum of poly(dA)·poly(dT).
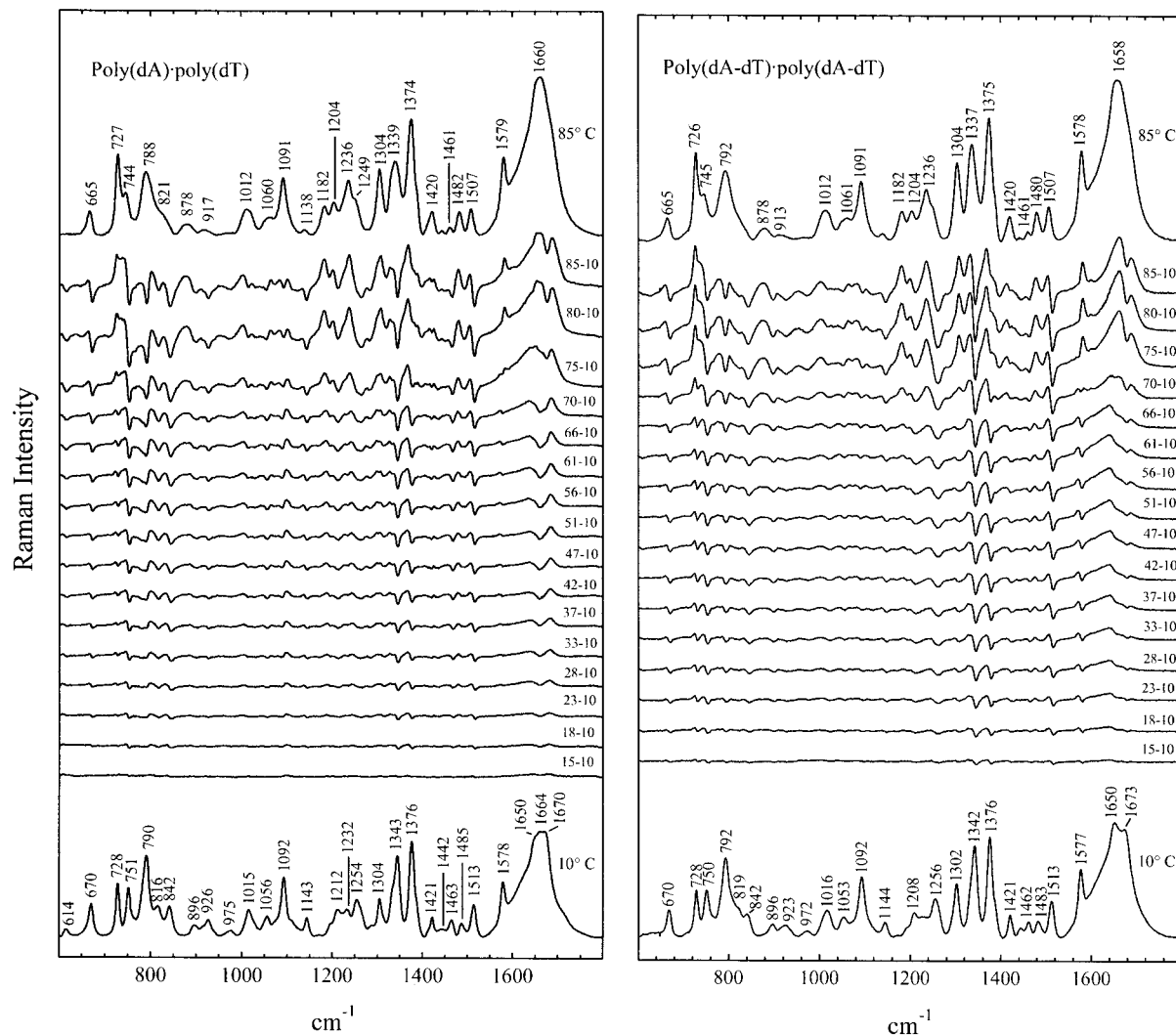
FIGURE 1   Left panel: Raman spectra of poly(dA)·poly(dT) in 100 m*M* NaCl solution, pH 7.0, at 10°C (bottom trace) and 85°C (top trace). Intermediate traces show the difference spectra computed with the higher temperature spectrum as minuend and the 10°C spectrum as subtrahend. Right panel: Corresponding Raman spectra of poly(dA-dT)·poly(dA-dT) at the same conditions given in the left panel. DNA concentration is 35 mg/mL in each case.

Corresponding data for double-helical poly(dA-dT)·poly(dA-dT) are shown in the right panel of Figure 1. Melting of poly(dA-dT)·poly(dA-dT) occurs in the interval 66–75°C with T_m = 71.4 ± 0.3°C, while poly(dA-dT)·poly(dA-dT) premelting occurs over the range 10–66°C.[12]

The results of Figures 1–4 (as well as other melting and premelting data not shown) are compiled in Table I, which also lists specific residue and vibrational assignments for the Raman bands. Assignments are based upon detailed analyses of related nucleic acids and nucleotides.[12,13,20,38–41] In Table I, the temperature-dependent change of a

Raman band between the lowest (either 10 or 15°C) and highest temperature (85°C) is characterized by two parameters: $\Delta\sigma$, the shift in wavenumber value, and $\Delta I_\sigma/I_\sigma$, the percent change in relative band intensity defined by Eq. (1):

$$\Delta I_\sigma/I_\sigma = 100(I_\sigma^{85} - I_\sigma)/I_\sigma \qquad (1)$$

Here, I_σ is the intensity of the band at wavenumber σ in the lower temperature spectrum, ΔI_σ is the change in band intensity between the lower temperature and 85°C, and the data are normalized using the 1092 cm^{-1} band of the PO$_2^-$ group.
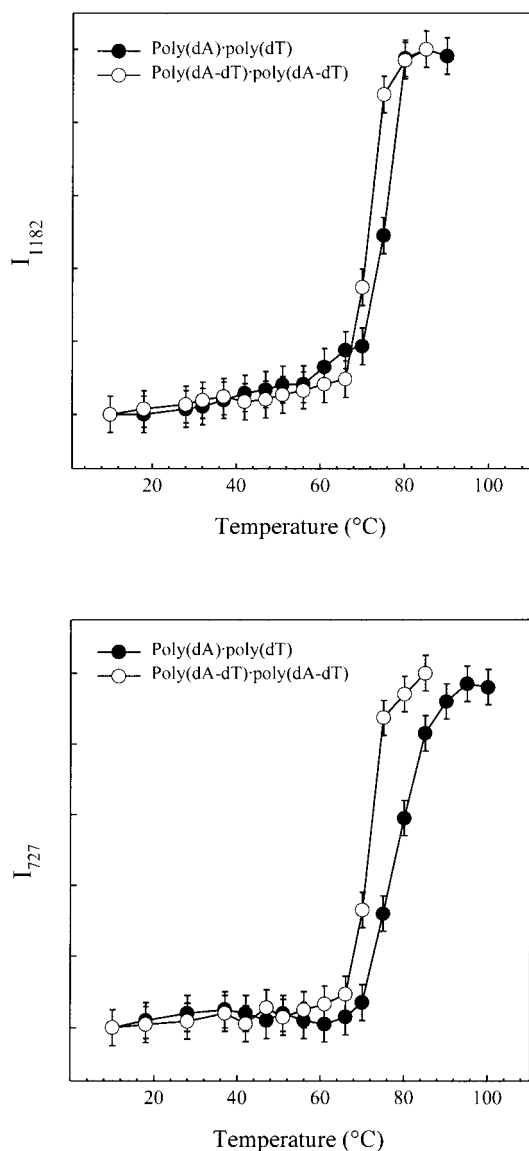
FIGURE 2 Top panel: Temperature dependence of the normalized Raman intensity at 1182 cm^{-1} (I_{1182}) in poly(dA)·poly(dT) (●) and (dA-dT)·poly(dA-dT) (○) over the range $10 < t < 85°C$. The increasing amplitude of I_{1182} with temperature is a quantitative measure of the extent of thymine unpairing and indicates a median melting temperature $T_m = 76.5 \pm 0.4°C$ for poly(dA)·poly(dT). Bottom panel: Temperature dependence of the normalized Raman intensity at 727 cm^{-1} (I_{727}) in poly(dA)·poly(dT) (●) and poly(dA-dT)·poly(dA-dT) (○) over the range $10 < t < 85°C$. The increasing amplitude of I_{727} with temperature is a quantitative measure of the extent of adenine unstacking. The slightly lower cooperativity and marginally higher apparent melting temperature suggested for poly(dA)·poly(dT) by the I_{727} plot compared with the I_{1182} plot (above) reflect the persistence of adenine base stacking in the separated poly(dA) strand.
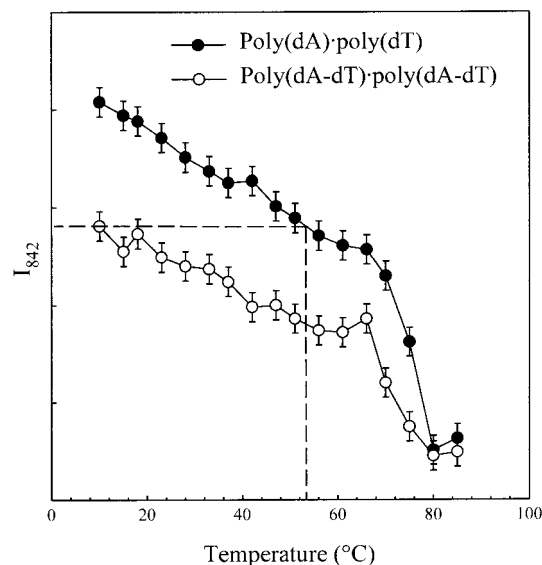
FIGURE 3 Temperature dependence of the normalized Raman intensity at 842 cm^{-1} (I_{842}) in poly(dA)·poly(dT) (●) and poly(dA-dT)·poly(dA-dT) (○) over the range $10 < t < 85°C$. The amplitude of I_{842} is a quantitative measure of ordered phosphodiester C5′–O5′–P–O3′–C3′ linkages in each DNA. The data show that the ordered backbone conformation of poly(dA)·poly(dT) is significantly more thermostable than that of poly(dA-dT)·poly(dA-dT) at all temperatures below complete melting (80°C). For example, the value of I_{842} for poly(dA-dT)·poly(dA-dT) at 10°C is comparable to that of poly(dA)·poly(dT) at 53°C (dashed horizontal line); also at 53°C, poly(dA-dT)·poly(dA-dT) maintains only about one-third of the backbone order of poly(dA)·poly(dT) (dashed vertical line).

Raman Signatures of Premelting and Melting Transitions of Poly(dA)·Poly(dT)

The top panel of Figure 5 compares Raman *difference* signatures for the melting (top trace) and premelting (bottom trace) transitions of poly(dA)·poly(dT). The two are strikingly dissimilar, indicating that very different types of structural changes take place during premelting and melting phases. A corresponding comparison for poly(dA-dT)·poly(dA-dT) is shown in the bottom panel of Figure 5, again demonstrating distinctively different structural changes for the premelting and melting transitions of this structure.

Figure 5 also shows that poly(dA)·poly(dT) and poly(dA-dT)·poly(dA-dT) exhibit dissimilar premelting signatures, particularly with respect to the amplitudes of their respective difference bands. This reflects primarily the fact that the two types of B-DNA have a significantly different Raman spectrum at low temperature (10–15°C). The distinguishing characteristics in low temperature spectra are gradually elimi-
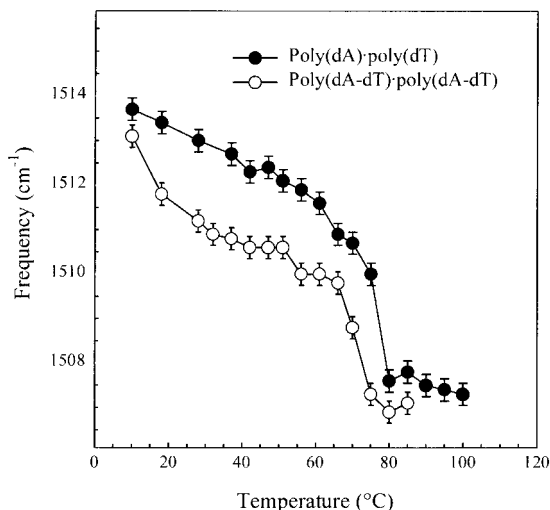
FIGURE 4 Temperature dependence of the center of the adenine Raman band near 1513 ± 2 cm^{-1} (σ_{1513}) in poly(dA)·poly(dT) (●) and poly(dA-dT)·poly(dA-dT) (○) over the range $10 < t < 85$°C. The decreasing wavenumber value of σ_{1513} with temperature is a measure of the decreasing extent of adenine N-acceptor hydrogen bonding.

nated as temperature is increased up to the premelting limit (data not shown). Virtually identical structural changes ensue as temperature is further increased through the melting phase, and thus poly(dA)·poly(dT) and poly(dA-dT)·poly(dA-dT) exhibit quite similar melting signatures.

Backbone Conformation

The definitive Raman marker of DNA secondary structure occurs in the spectral region $750-850$ cm^{-1}. The band is assigned to a bond-stretching vibration localized in the phosphodiester C5′–O5′–P–O3′–C3′ network, a group of linkages sensitive to the conformation of the DNA backbone.[17,19,23,25,39–41] The Raman marker of "canonical" B-form geometry is generally observed at 835 ± 1 cm^{-1} in genomic B-DNA of mixed base composition. However, in GC-rich polynucleotide duplexes, such as poly(dG-dC)·poly(dG-dC) (dC: deoxycytidine; dG: deoxyguanosine), the corresponding marker is observed near 829 ± 1 cm^{-1}; conversely in AT-rich polynucleotide duplexes, including both poly(dA-dT)·poly(dA-dT) and poly(dA)·poly(dT), the marker is observed near 841 ± 1 cm^{-1}.[12,20,39] These polynucleotide duplexes, though members of the B family of DNA structures, are minor variants of "canonical" B-DNA in the sense that they exhibit certain properties—including Raman markers of phosphodiester geometry—differing somewhat from those of genomic B-DNA. The de-

pendence of Raman markers of phosphodiester geometry on base composition has been attributed to subtle differences in the conformations of the C5′–O5′–P–O3′–C3′ networks in AT and GC sequences of DNA[22] and may reflect nonidentical groove dimensions.[42]

The normalized intensity of the 842 cm^{-1} band (I_{842}) of poly(dA)·poly(dT) is plotted as a function of temperature in Figure 3, where it is compared with the corresponding plot for poly(dA-dT)·poly(dA-dT). Interestingly, at every temperature below the onset of melting, I_{842} is greater for poly(dA)·poly(dT) than for poly(dA-dT)·poly(dA-dT). For example, the I_{842} amplitude that is observed in the A-tract structure at 53°C is not observed in the alternating A·T/T·A structure unless the temperature is as low as 10°C. Indeed, the local backbone conformation (C5′–O5′–P–O3′–C3′ geometry) specific to this B-DNA variant is more prevalent in poly(dA)·poly(dT) than in poly(dA-dT)·poly(dA-dT) at every temperature below the onset of melting. This geometry is believed to be characterized by α and ζ torsions in the *gauche*$^-$ (g^-) and *trans* (t) orientations, respectively.[12] The premelting-induced attenuation of I_{842} without corresponding changes in Raman bands of the bases (cf. top and bottom panels of Figure 2) demonstrates a significant change in backbone geometry without a concomitant change in either base stacking or Watson–Crick pairing. This appears to be the case for both poly(dA)·poly(dT) and poly(dA-dT)·poly(dA-dT), although the effect is much more pronounced in the former duplex.

Watson–Crick Pairing and Base Stacking

The top panel of Figure 2 compares the temperature-dependent intensity of the Raman band at 1182 cm^{-1} (I_{1182}) of poly(dA)·poly(dT) with that of poly(dA-dT)·poly(dA-dT). The 1182 cm^{-1} band, assigned to dT,[21] is diagnostic of the unpaired thymidine residue.[12] The band owes its intensity to coupling between a ring-stretching vibration of the base and a methylene wagging vibration of the deoxyribosyl C2′H$_2$ group. This vibrational coupling is conformation sensitive and is significant only when thymidine is unpaired. When paired with dA, the thymidine base and C2′H$_2$ modes uncouple and the 1182 cm^{-1} band is supplanted by a pure thymine ring mode at 1204 cm^{-1} (Table I).[21] Because vibrational coupling is significant *only when thymidine is unpaired*, the percent change in Raman band intensity is a quantitative measure of the distribution of dT between paired and unpaired states.[12] The data of Figure 2 (top panel) show

Table I   Assignments and Temperature Dependence of Raman Bands of Poly(dA-dT)·Poly(dA-dT) and Poly(dA)·Poly(dT)

Poly(dA-dT)·Poly(dA-dT)					Poly(dA)·Poly(dT)			
σ^a	Assignment[b]	I^c	$\Delta\sigma^d$	$\Delta I/I$ (%)[e]	σ^a	I^c	$\Delta\sigma^d$	$\Delta I/I$ (%)[e]
668	dT, dA	4.5	−3	−11.5	670	5.4	−5	−21.7
728	dA	7.8	−2	93.1	728	8.9	−1	55.8
750	dT	7.8	−5	4.0	751	8.2	−7	−9.2
792[f]	bk (OPO st)	13.2	0	−10.2	790	13.6	−2	−20.2
819	bk (OPO st)	5.1	U	U	816	5.1	U	U
842	bk (OPO st)	3.8	U	**−56.3**	842	5.1	U	**−67.6**
896	C2′H$_2$ rk	2.2	−18	9.9	896	1.9	−18	7.4
923	d (ring st)	1.9	−10	−44.7	926	2.8	−9	−62.5
972	T (C6H op df)	1.1	U	−44.0	975	0.9	U	−46.2
1016	T (CH$_3$ ip rk)	4.5	−4	18.2	1015	4.5	−3	1.5
1053	d (CO st)	3.4	0	5.7	1056	3.4	0	−12.2
1061	d (CO st)	4.0	U	U	*1060*	3.2	U	U
1092	bk (PO$_2^-$ st)	10.0	0	0.0	1092	10.0	0	0.0
1144	T	2.5	−4	−43.7	1143	3.1	−5	3.1
1182	dT	5.1	U	(∞)	*1182*	5.0	U	(∞)
1193s	C2′H$_2$ wg	1.7	U	125.1	1196	2.3	U	U
1208	dT, A	4.1	−4	24.8	1212	4.6	−8	25.4
1236	T	8.7	U	**158.5**	1232	4.6	+4	**109.0**
1256	A, T	6.4	−5	−7.9	1254	6.3	−5	3.3
1302	A, T	9.0	+2	46.4	1304	6.4	0	77.7
1342	A	15.2	−5	7.4	1343	13.8	−4	−6.5
1376	T (CH$_3$ df), A	16.8	−1	23.6	1376	16.3	−2	23.3
1420	A, C5′H$_2$ df	3.8	0	10.6	1421	3.3	−1	31.3
1444	C5′H$_2$ df	1.6	−2	−55.7	1442	1.3	+1	−26.3
1462	C2′H$_2$ df	2.6	−1	−34.4	1463	2.8	−2	−46.3
1483	A, T	2.8	−3	74.6	1485	2.2	−3	90.6
1512	A	6.1	−5	−3.5	1513	5.4	−6	−13.9
1577	A (ring st; N6H$_2$ df)	11.4	+1	33.9	1578	9.4	+1	44.9
1650[g]	C4=O/C5=C6 st	19.2	U	37.3	1650[g]	17.2	U	U
1673[g]	C4=O/C5=C6 st	18.1	U	26.4	1670[g]	17.9	U	U

[a] Raman wavenumber (cm^{-1} units) in the spectrum of the duplex at 10°C. Entries in italics indicate bands observed only for the dissociated single strands ($t > T_m$).

[b] From Refs. 12 and 47 and citations therein. Abbreviations: dA, deoxyadenosine; dT, thymidine; A, adenine; T, thymine; bk, backbone; d, deoxyribose; st, stretch; df, deformation; rk, rock; wg, wag; op, out-of-plane; ip, in-plane.

[c] Intensity relative to an arbitrary value of 10.0 for the 1092 cm^{-1} band.

[d] Raman wavenumber shift (cm^{-1} units) observed with melting. U indicates an unmeasurable quantity.

[e] Percent relative intensity change with melting [Eq. (1)]. The band at 1182 cm^{-1} has zero intensity at 10°C (see text). Bold type indicates the maximal and minimal intensity changes observed.

[f] A thymine ring mode is also expected near 785 cm^{-1} and may contribute to the observed band intensity.

[g] The C2=O stretching mode of thymine and additional factors complicate the assignment of peaks observed near 1650 and 1670 cm^{-1}, as discussed in the text. See also Table II (1661 and 1681 cm^{-1}).

that unpairing of dA and dT is highly cooperative in both the A-tract structure [poly(dA)·poly(dT)] and alternating A·T/T·A structure [poly(dA-dT)· poly(dA-dT)], and that the T_m values are separated by about 5°C, with the A-tract structure being more thermostable.

The bottom panel of Figure 2 demonstrates the temperature dependence of adenine base unstacking, as monitored by the intensity increase (recovery of Raman hypochromism) in the 727 cm^{-1} band of dA residues.[12,16,43] I_{727} shows that adenine unstacking is highly cooperative in both the A-tract and alternating A·T/T·A structures, with T_m again higher for the former structure. The results of Figures 2 and 3 contrast the cooperativity of melting vs the noncooperativity of premelting for both poly(dA)·poly(dT) and poly(dA-dT)·poly(dA-dT).
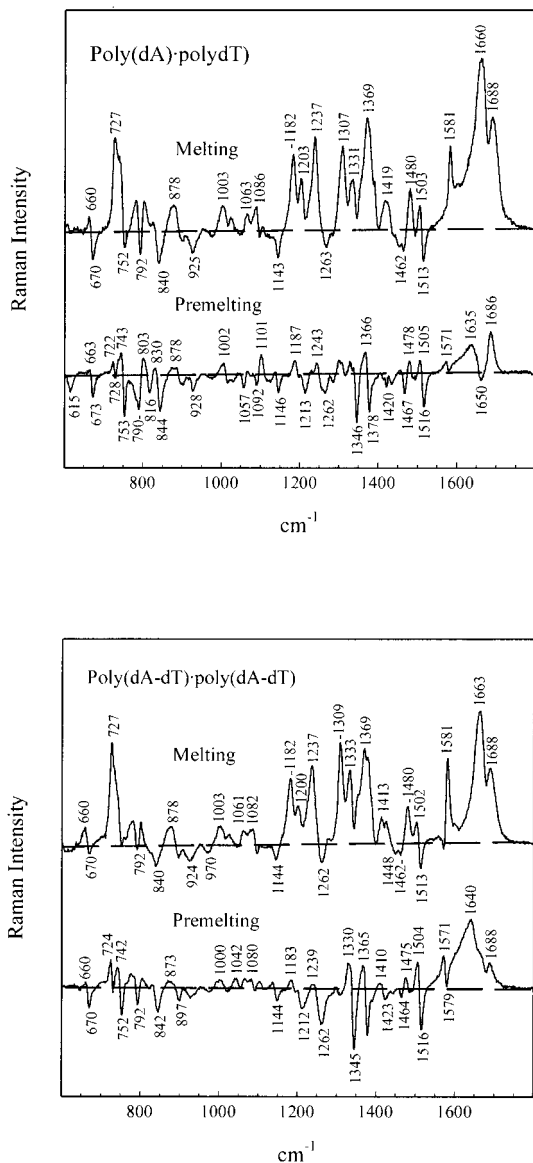
FIGURE 5 Top panel: Raman difference spectra demonstrating premelting and melting transitions of poly(dA)·poly(dT) in 100 m*M* NaCl solution, pH 7. The Raman premelting and melting signatures are defined as the difference spectra between 66 and 10°C and between 80 and 66°C, respectively. Bottom panel: Raman difference spectra demonstrating premelting (between 66 and 10°C) and melting (between 75 and 66°C) transitions of poly(dA-dT)·poly(dA-dT) in 100 m*M* NaCl solution, pH 7.

Comparison of Premelting in Poly(dA)·Poly(dT) and Poly(dA-dT)·Poly(dA-dT)

Deoxynucleoside and Backbone Conformations.
Although Raman spectral changes with premelting are generally different in poly(dA)·poly(dT) and poly(dA-dT)·poly(dA-dT) (Figure 5), many similar wavenumber shifts are observed for the two structures. One interpretation for the Raman band shifts $670 \rightarrow 660$ (dT), $728 \rightarrow 722$ (dA), $753 \rightarrow 743$ (dT), and $1346 \rightarrow 1330 \ cm^{-1}$ (dA) is a change in deoxynucleoside sugar pucker from the C2′-*endo/anti* family to the C3′-*endo/anti* family.[12–14] A rough quantitative estimate consistent with the data is that approximately one-third of the deoxynucleosides are converted to the C3′-*endo* conformation in premelted poly(dA)·poly(dT) at 70°C.[12] The premelting shift in the phosphodiester marker ($842 \rightarrow \sim 835 \ cm^{-1}$) suggests that the backbone conformation specific to AT-rich DNA at low temperature is altered in favor of the canonical B conformation ($834 \ cm^{-1}$ marker) associated with genomic DNA of mixed base composition.[30] Thus, the shift of the $842 \ cm^{-1}$ marker to lower wavenumber with increasing temperature can be interpreted as a widening of the narrow minor groove of AT-rich DNA toward the groove size of genomic B-DNA.[22]

Interbase Hydrogen Bonding. The Raman band shifts $1262 \rightarrow 1243$ (dA), $1378 \rightarrow 1366$ (dT), $1516 \rightarrow 1505$ (dA), and $1579 \rightarrow 1571 \ cm^{-1}$ (dA) are common to the two duplexes and all are associated with elimination of hydrogen bonding at base sites. Because Watson–Crick pairing remains intact through the premelting phase (Figure 2, top), the ruptured hydrogen bonds must involve either interbase interactions of a non-Watson–Crick type, such as bifurcated hydrogen bonding,[3] or interactions of base sites with other agents, such as water molecules or ions. Further discussion is given below.

Adenine Marker at 1513 cm^{-1}. Surprisingly, the adenine marker at $1513 \ cm^{-1}$ exhibits different premelting behavior in poly(dA)·poly(dT) and poly(dA-dT)·poly(dA-dT), as shown in Figure 4. Whereas poly(dA)·poly(dT) premelting is characterized by a monotonic and approximately linear wavenumber decrease between 10 and 60°C, poly(dA-dT)·poly(dA-dT) shows a large decrease between 10 and 30°C, followed by a more gradual decrease between 30 and 60°C. These results imply that hydrogen-bonding interaction of the applicable dA site is significantly more thermostable in poly(dA)·poly(dT) than in poly(dA-dT)·poly(dA-dT). On the basis of isotopic substitution experiments, the $1513 \ cm^{-1}$ band of dA has been assigned to a vibration localized in the imidazolium ring of adenine.[44] Polarized Raman measurements demonstrate a large anisotropy in the Raman tensor, implying that the $1513 \ cm^{-1}$ band may be responsive to hydrogen-bond

formation not only at N7,[45] but also at N1 and/or N3.[18] Accordingly, it is reasonable to conclude that the observed difference in premelting behavior of 1513 cm^{-1} markers of poly(dA)·poly(dT) and poly(dA-dT)·poly(dA-dT) reflects stronger hydrogen bonding of N1, N3, and/or N7 acceptor sites of the former.

Thymine Markers Near 1600–1700 cm^{-1}. The most striking spectral difference between poly(dA)·poly(dT) and poly(dA-dT)·poly(dA-dT) occurs in the interval 1600–1700 cm^{-1}, where thymine carbonyl (C2=O and C4=O) and ring double-bond (C5=C6) stretching vibrations are the expected major contributors.[7,13,21] Assignment of the bands to specific C=O and C=C stretching coordinates is not trivial, but is important for interpreting hydrogen-bonding interactions in the two duplexes. In the 10°C spectra of Fig. 1, there appear to be three distinct Raman bands for poly(dA)·poly(dT), at 1650, 1664 and 1670 cm^{-1}, but only two for poly(dA-dT)·poly(dA-dT), at 1650 and 1673 cm^{-1}. Additional bands ca. 1635–1640 and 1686 cm^{-1} emerge in the premelting difference signatures of Figure 5. In a recent analysis of ultraviolet-resonance Raman (UVRR) spectra of poly(dA)·poly(dT), bands at 1650 and 1679 cm^{-1} were assigned, respectively, to in-phase and out-of-phase stretching vibrations of coupled C2=O and C4=O groups, whereas a band near 1665 cm^{-1} was assigned to the C5=C6 stretch.[7] The 1679 cm^{-1} UVRR band exhibits the largest premelting perturbation (a shift to 1686 cm^{-1} at 55°C). An alternative and more comprehensive assignment scheme has been developed from detailed analysis of Raman, UVRR and infrared spectra and *ab initio* calculations on thymine and isotopically labeled analogs.[46] Thus, thymine bands near 1650 and 1670 cm^{-1} were assigned, respectively, to out-of-phase and in-phase stretching vibrations of coupled C4=O and C5=C6 groups, and the thymine band of highest wavenumber value (near 1680–1690 cm^{-1} for thymine residues of DNA) was assigned to the C2=O stretch. In this scheme, the definitive UVRR premelting shift of poly(dA)·poly(dT), i.e., 1679 → 1686 cm^{-1},[46] cannot reasonably be attributed to the rupture of bifurcated hydrogen bonds along the major groove (i.e., involving C4=O sites), because the band in question is more appropriately assigned to C2=O, which is situated along the minor groove.

Figure 6 compares on an expanded scale the strikingly different temperature-dependent Raman profiles in the 1500–1800 cm^{-1} interval of poly(dA)·poly(dT) and poly(dA-dT)·poly(dA-dT). The data demonstrate different premelting shifts for the respective C2=O markers, i.e., 1661 → 1684 cm^{-1} in poly(dA)·poly(dT)

Poly(dA)·poly(dT)   Poly(dA-dT)·poly(dA-dT)
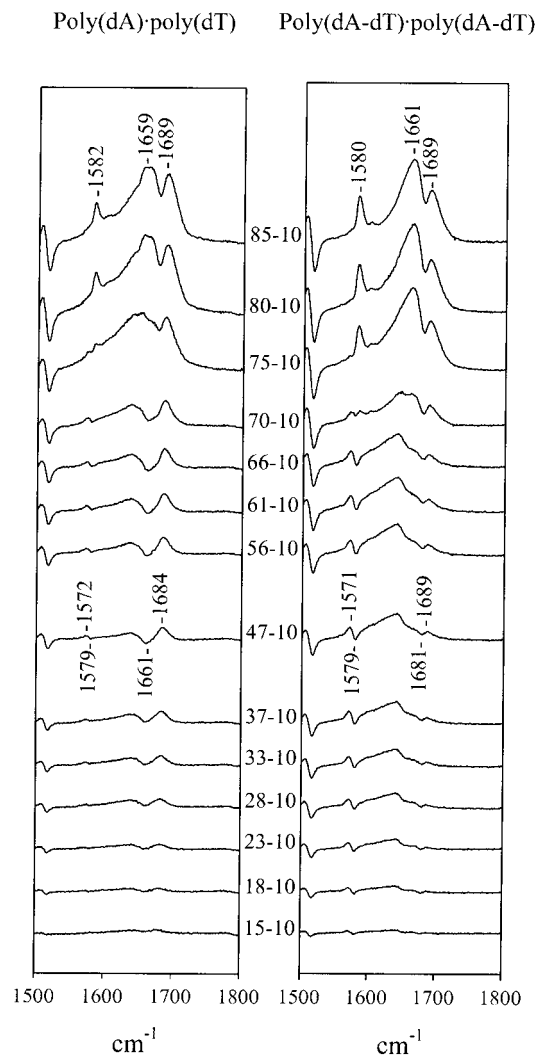
FIGURE 6 Left panel: Raman difference spectra of poly(dA)·poly(dT) in the interval 1500–1800 cm^{-1}, showing temperature-dependent changes in bands due to thymine double-bond stretching modes. Right panel: Corresponding data for poly(dA-dT)·poly(dA-dT). All data are from spectra of Figure 1.

vs 1681 → 1689 cm^{-1} in poly(dA-dT)·poly(dA-dT). This suggests much stronger hydrogen bonding of C2=O in the low-temperature structure of poly(dA)·poly(dT) (1661 cm^{-1} marker) than in that of poly(dA-dT)·poly(dA-dT) (1681 cm^{-1} marker). The greater hydrogen bonding strength exhibited by the C2=O carbonyl of poly(dA)·poly(dT) may contribute to the greater thermostability (higher T_m) of this homopurine/homopyrimidine duplex. In any case, we interpret the results as evidence that the two AT-rich DNA structures are distinguished by very different hydrogen-bonding characteristics of C2=O acceptors situated along their respective minor grooves.

Another interesting feature of Figure 6 is the different premelting profiles observed for 1578 cm^{-1} bands in poly(dA)·poly(dT) and poly(dA-dT)·poly(dA-dT). The band is unperturbed by poly(dA)·poly(dT) premelting, but substantially perturbed by poly(dA-dT)·poly(dA-dT) premelting. The Raman marker at 1578 cm^{-1} is due to a ring mode of adenine that includes a contribution from the exocyclic amino group (N6H$_2$).[12,47] Studies of adenosine model compounds in polar and apolar solvents confirm that the band is sensitive to changes in N6—H hydrogen bonding.[18,48] Accordingly, one interpretation of the present results is that N6—H···O4 bonding (A·T pairing) is significantly more thermostable in the homopolymer duplex. This interpretation is consistent with proposed bifurcated hydrogen bonding in A-tracts.[3]

Comparison of Melting in Poly(dA)·Poly(dT) and Poly(dA-dT)·Poly(dA-dT)

Figure 5 reveals that the melting signatures of poly(dA)·poly(dT) and poly(dA-dT)·poly(dA-dT) are qualitatively very similar. Both are dominated by Raman intensity increases (near 727, 1200, 1237, 1309, 1333, 1369, 1480, 1581, 1660, and 1688 cm^{-1}) that reflect primarily base unstacking and the recovery of Raman hypochromism.[12,16,43] Several intensity changes (bands at 1182, 1663, and 1688 cm^{-1}) are also associated with the rupture of Watson–Crick hydrogen bonding.

An unfortunate consequence of the recovery of Raman hypochromism in intrinsically intense Raman bands is the obscuration of underlying weaker Raman bands. For example, the recovery of hypochromism at ~1578 cm^{-1} obscures the region 1570–1580 cm^{-1} and prevents continued monitoring of the distinctively different premelting profiles of poly(dA)·poly(dT) and poly(dA-dT)·poly(dA-dT) ca. 1578 cm^{-1}. Many similar interference effects occur in the 1150–1400 cm^{-1} interval.

DISCUSSION

Premelting

Premelting is detected by Raman spectroscopy in both poly(dA)·poly(dT) and poly(dA-dT)·poly(dA-dT), consistent with earlier CD studies.[2,5,11] The present results also support the previous finding by UVRR spectroscopy[7] of premelting in poly(dA)·poly(dT). The inability to detect premelting in poly(dA-dT)·poly(dA-dT) by UVRR spectroscopy[7] is not consistent with either earlier CD studies or present results, and presumably reflects the low signal-to-noise quality of the previously reported UVRR data as well as the narrower focus of resonance Raman vis-à-vis off-resonance Raman as a spectroscopic probe. For example, UVRR spectroscopy of DNA is largely transparent to structural changes localized in the deoxyribosyl-phosphate backbone, whereas such conformational changes are reported by the off-resonance Raman method.[38]

Premelting signatures of both poly(dA)·poly(dT) and poly(dA-dT)·poly(dA-dT) are dominated by Raman wavenumber shifts, rather than the intensity changes that dominate the corresponding melting signatures (Figure 5). This indicates that structural changes occurring during the premelting phase involve relatively minor readjustments in backbone conformation and hydrogen bonding, rather than rupture of base pairing, base unstacking and strand separation. Several major differences are apparent between the premelting signatures of poly(dA)·poly(dT) and poly(dA-dT)·poly(dA-dT). For example, Raman features associated with the non-Watson–Crick hydrogen bonding of adenine (i.e., involving acceptor sites N1, N3, and/or N7) are more resistant to premelting in poly(dA)·poly(dT) than in poly(dA-dT)·poly(dA-dT). Thus, although adenine acceptor-site hydrogen bonding is present in both duplexes at lower temperatures, the interactions are more thermostable in poly(dA)·poly(dT). This is in accord with the enhanced stability of the low-temperature backbone conformation of poly(dA)·poly(dT) compared to that of poly(dA-dT)·poly(dA-dT), as monitored by the 842 cm^{-1} Raman marker (Figure 3). Another major difference in premelting involves Raman bands associated with the thymine 2C=O group. In poly(dA)·poly(dT) we observe a premelting shift of the carbonyl Raman marker from 1661 to 1681 cm^{-1}. This reflects rupture of 2C=O hydrogen bonding as temperature is increased through the premelting phase. In the case of poly(dA-dT)·poly(dA-dT) the effect is much less pronounced, indicating much weaker 2C=O hydrogen-bonding interaction. These results show that the two AT-rich DNA structures are distinguished by different hydrogen-bonding characteristics of their respective thymine C2=O acceptor and adenine N-acceptor sites. With the exception of N7, such sites line the minor-groove. A third significant difference between premelting transitions in poly(dA)·poly(dT) and poly(dA-dT)·poly(dA-dT) occurs in the Raman marker at 1578 cm^{-1}, which we interpret as diagnostic of different thermostabilities of base pairing in the two duplexes.

During premelting, the backbone Raman markers of both poly(dA)·poly(dT) and poly(dA-dT)·poly(dA-dT)

shift noncooperatively from 842 to ~835 cm^{-1}, i.e., from the position diagnostic of the structure of AT-rich DNA to the position characteristic of mixed sequence genomic DNA. The midpoint of the noncooperative transition in poly(dA)·poly(dT) is 35 ± 5°C, which is consistent with values reported by others for this transition.[2,6,8] The present findings are consistent with CD spectra, DNase-I digestion and daunomycin-binding studies of poly(dA)·poly(dT) by Herrera and Chaires,[2] who proposed a structure adjustment from a variant of the form to the canonical B form during premelting. Our results are also in accord with the finding that poly(dA)·poly(dT) can be incorporated into stable nucleosomes only at temperatures higher than required for other polynucleotide duplexes.[49] Finally, we note that the temperature profile observed for the 1182 cm^{-1} marker of poly(dA-dT)·poly(dA-dT) (Figure 2, top panel) implies that hairpin intermediates[50,51] are not formed during the premelting phase, which is consistent with previous spectroscopic studies.[5,35]

Melting

DNA base unstacking and unpairing transitions during strand separation are highly cooperative phenomena. Such cooperativity is manifested in sharp melting profiles for Raman bands sensitive to certain interbase interactions (Figure 2). Importantly, similar cooperativity is observed for the 842 cm^{-1} backbone marker during the melting phase, but not during the premelting phase (Figure 3). These results indicate that strand separation leads to a cooperative "collapse" of the C5′–O5′–P–O3′–C3′ geometry associated with B-DNA. Subsequent to strand separation the ~835 cm^{-1} marker of the premelted duplex is replaced by a broad band centered near 878 cm^{-1} (Figure 1). We assign the 878 cm^{-1} band as a marker of the C5′–O5′–P–O3′–C3′ structure (or group of closely related structures) associated with the melted polynucleotide single strands. Very likely, the 878 cm^{-1} band is diagnostic of a broad range of phosphodiester bond torsions.

Minor-Groove Hydrogen Bonding

The Raman spectra of poly(dA)·poly(dT) and poly(dA-dT)·poly(dA-dT) provide evidence that hydrogen bonding occurs at sites of adenine (N acceptors) and thymine (C2═O acceptor) in addition to the sites involved in Watson–Crick base pairing. Such hydrogen bonding, which is much more robust in poly(dA)·poly(dT) than in poly(dA-dT)·poly(dA-dT), is gradually eliminated as temperature is increased

through the premelting phase. The Raman spectra do not identify the hydrogen-bond donor groups that may interact with either the C2═O acceptor site of thymine or the N-acceptor site(s) of adenine. Nevertheless, the participation of C2═O implicates the *minor* groove as the locus of hydrogen bonding interactions that stabilize the secondary structure of AT-rich DNA. Minor-groove involvement is also consistent with the adenine Raman markers.

Previously, the Raman 1661 → 1681 cm^{-1} shift (observed by UVRR) had been attributed to the rupture of bifurcated hydrogen bonds involving C4═O sites situated along the *major* groove of the poly(dA)·poly(dT) duplex.[7] In the present work, we assign the Raman marker in question to C2═O, rather than C4═O, which is consistent with a very large body of experimental and theoretical vibrational analyses.[46] The present results do not preclude bifurcation in poly(dA)·poly(dT), as originally proposed on the basis of x-ray crystallography of a related oligonucleotide.[3] Rather, the present findings suggest that bifurcated hydrogen bonding of C4═O is not monitored by the 1661 cm^{-1} marker and is not necessarily eliminated by heating through the premelting phase. This conclusion is also supported by the resistance of the 1578 cm^{-1} marker of poly(dA)·poly(dT) to changes during the premelting transition.

Spine of Hydration

Although hydration is important for the stabilization of all B-DNA sequences,[52,53] a unique and highly ordered "spine of hydration" has been identified in the minor groove of DNA containing adenine tracts.[32,54–59] The specifically bound water molecules of A-tract DNA duplexes exhibit much slower exchange rates than water molecules in general, including water associated with DNA single strands.[60–63] Recent osmotic stress measurements[64] indicate that melting of poly(dA)·poly(dT) releases ~4 such specifically bound water molecules per base pair, in reasonably good agreement with x-ray crystal structures showing ~5 hydrogen-bonded water molecules per DNA base pair.[65] The Raman wavenumber shifts that characterize the premelting signatures of AT-rich DNA may reflect the disruption of specifically bound water molecules. While the data of Figure 5 are consistent with bound water for both poly(dA)·poly(dT) and poly(dA-dT)·poly(dA-dT), the differences observed between the two duplexes are compatible with much stronger minor-groove binding of H_2O in poly(dA)·poly(dT) than in poly(dA-dT)·poly(dA-dT). The Raman results are also consistent with thermodynamic analyses suggesting that the probability of

Table II   Raman Markers Diagnostic of Structural Features of AT-Rich DNA

Marker (cm^{-1})	Structural Significance
842	Indicator of the phosphodiester C5′—O5′—P—O3′—C3′ conformation (g^-, t) specific to the narrow minor-groove variant of B-DNA
878	Indicator of the phosphodiester C5′—O5′—P—O3′—C3′ conformation of single-stranded (melted) poly(dA), poly(dT), and poly(dA-dT)
1182	Indicator of unpaired thymine residues
1262	Indicator of adenine interaction common to both poly(dA)·poly(dT) and poly(dA-dT)·poly(dA-dT); shifts to 1243 cm^{-1} with premelting
1378	Indicator of thymine interaction common to both poly(dA)·poly(dT) and poly(dA-dT)·poly(dA-dT); shifts to 1366 cm^{-1} with premelting
1513	Indicator of non-Watson–Crick hydrogen bonding of adenine N-acceptor sites (probably N1 and/or N3)
1578	Indicator of adenine $N6H_2$ hydrogen-bonding interactions in AT-rich DNA; shifts to lower wavenumber (ca. 1575 cm^{-1}) with premelting; returns to higher wavenumber (ca. 1578 cm^{-1}) with melting
1661	Indicator of non-Watson–Crick hydrogen bonding of the thymine C2=O site; shifts to ~1684 cm^{-1} in premelted poly(dA-dT)·poly(dA-dT)
1681	Indicator of weak (or negligible) thymine C2=O hydrogen bonding; shifts to ~1689 cm^{-1} in premelted poly(dA-dT)·poly(dA-dT)

disruption of the spine of hydration in A-tract DNA increases with temperature.[66,67]

CONCLUDING SUMMARY

The salient results and conclusions of this study can be summarized as follows:

1. Poly(dA)·poly(dT) exhibits a secondary structure that is a minor variant of canonical B-DNA. Although dA and dT residues of this structure adopt the C2′-*endo/anti* conformation found in B-DNA, the local geometry of nucleotide phosphodiester C5′–O5′–P–O3′–C3′ linkages differs from that of B-DNA. A similar (though much less thermostable) secondary structure is observed for poly(dA-dT)·poly(dA-dT). Because the local C5′–O5′–P–O3′–C3′ geometry specific to nucleotides of these AT-rich DNAs results in a globally narrow minor groove, the defining Raman marker (842 cm^{-1}) can be considered diagnostic of such a global structure.

2. Poly(dA)·poly(dT) and poly(dA-dT)·poly(dA-dT) exhibit distinctive and noncooperative premelting transitions in the range $10 < t < 70°C$. The premelted structures are characterized by Raman markers of backbone geometry similar to those of canonical B-DNA. However, a substantial proportion (roughly one-third) of deoxynucleosides in the pre-

melted structures appear to undergo a conformational change from C2′-*endo/anti* at 10°C to C3′-*endo/anti* at ~70°C.

3. The premelting Raman signatures of poly(dA)·poly(dT) and poly(dA-dT)·poly(dA-dT) can be rationalized as representative of the destabilization of hydrogen-bonding interactions of adenine and thymine base sites that line the *minor* groove. Such minor-groove interactions are much more prevalent and thermostable in poly(dA)·poly(dT) than in poly(dA-dT)·poly(dA-dT).

4. Premelting in poly(dA)·poly(dT) is also distinguished from that of poly(dA-dT)·poly(dA-dT) by more robust N6–H · · · O4 hydrogen bonding. This may reflect stabilization conferred to A·T pairs of poly(dA)·poly(dT) through bifurcated hydrogen bonding, as proposed in the A-tract oligonucleotide, d(CGCAAAAAA-GCG)·d(CGCTTTTTTGCG).[3]

5. Above 70°C, poly(dA)·poly(dT) and poly-(dA-dT)·poly(dA-dT) exhibit similar cooperative melting transitions, characterized by T_m values of 76.5 and 71.4 °C, respectively.

6. Although definitive Raman markers of bifurcated hydrogen bonding in poly(dA)·poly(dT) have not yet been identified, the resistance of the 1578 cm^{-1} adenine marker to premelting may signal a stabilizing effect of bifurcated hydrogen bonds.

7. Raman markers diagnostic of key structural features of AT-rich DNA are listed in Table II.

REFERENCES

1. Hagerman, P. J. Nature 1986, 321, 449–450.
2. Herrera, J. E.; Chaires, J. B. Biochemistry 1989, 28, 1993–2000.
3. Nelson, H. C. M.; Finch, J. T.; Luisi, B.; Klug, A. Nature 1987, 330, 221–226.
4. Crothers, D. M.; Haran, T. E.; Nadeau, J. G. J Biol Chem 1990, 265, 7093–7096.
5. Gennis, R. B.; Cantor, C. R. J Mol Biol 1971, 65, 381–399.
6. Chan, S. S.; Breslauer, K. J.; Hogan, M. E.; Kessler, R. H.; Austin, J.; Ojemann, J. M.; Passner, J. M.; Wiles, N. C. Biochemistry 1990, 29, 6161–6171.
7. Chan, S. S.; Austin, R. H.; Murkerji, I.; Spiro, T. G. Biophys J 1997, 72, 1512–1520.
8. Chan, S. S.; Breslauer, K. J.; Austin, R. H.; Hogan, M. E. Biochemistry 1993, 32, 11776–11784.
9. Haran, T. E.; Kahn, J. D.; Crothers, D. M. J Mol Biol 1994, 244, 135–143.
10. Diekmann, S. Nucleic Acids Res 1987, 15, 247–265.
11. Delrow, J. J.; Heath, P. J.; Fujimoto, B. S.; Schurr, J. M. Biopolymers 1998, 45, 503–515.
12. Movileanu, L.; Benevides, J. M.; Thomas, G. J., Jr. J Raman Spectrosc 1999, 30, 637–649.
13. Thomas, G. J., Jr.; Benevides, J. M. Biopolymers 1985, 24, 1101–1105.
14. Katahira, M.; Nishimura, Y.; Tsuboi, M.; Sato, T.; Mitsui, Y.; Iitaka, Y. Biochim Biophys Acta 1986, 867, 256–267.
15. Loprete, D. M.; Hartman, K. A. Bioploymers 1990, 30, 753–761.
16. Erfurth, S. C.; Peticolas, W. L. Biopolymers 1975, 14, 247–264.
17. Small, E. W.; Peticolas, W. L. Biopolymers 1971,10, 1377–1416.
18. Toyama, A.; Takeuchi, H.; Harada, H. J Mol Struct 1991, 242, 87–98.
19. Erfurth, S. C.; Kiser, E. R.; Kiser, J.; Peticolas, W. L. Proc Natl Acad Sci USA 1972, 69, 938–941.
20. Duguid, J. G.; Bloomfield, V. A.; Benevides, J. M.; Thomas, G. J., Jr. Biophys J 1996, 71, 3350–3360.
21. Tsuboi, M.; Komatsu, M.; Hoshi, J.; Kawashima, E.; Sekine, T.; Ishido, Y.; Russell, M. P.; Benevides, J. M.; Thomas, G. J., Jr. J Am Chem Soc 1997,119, 2025–2032.
22. Thomas, G. J., Jr.; Benevides, J. M.; Prescott, B. In Biomolecular Stereodynamics; Sarma, R. H., Sarma, M. H., Eds.; Adenine Press/Guilderland: New York, 1986; pp 227–253.
23. Small, E. W.; Peticolas, W. L. Biopolymers 1971, 10, 69–88.
24. Guan, Y.; Benevides, J. M.; Gao, Y. G.; Wang, A. H. J.; Thomas, G. J., Jr. Nucleic Acids Res 1998, 26, 3892–3899.
25. Guan, Y.; Thomas, G. J., Jr. Biopolymers 1996, 39, 813–835.
26. Patapoff, T. W.; Thomas, G. A.; Wang, Y.; Peticolas, W. L. Biopolymers 1988, 27, 493–507.
27. Thomas, G. A.; Peticolas, W. J Am Chem Soc 1983, 105, 993–996.
28. Thomas, G. J., Jr.; Barylski, J. Appl Spectrosc 1970, 24, 463–464.
29. Dong, J.; Dinakarpandian, D.; Carey, P. R. Appl Spectrosc 1998, 52, 1117–1122.
30. Deng, H.; Bloomfield, V.; Benevides, J. M.; Thomas, G. J., Jr. Biopolymers 1999, 50, 656–666.
31. Duguid, J. G.; Bloomfield, V. A.; Benevides, J. M.; Thomas, G. J., Jr. Biophys J 1995, 69, 2623–2641.
32. Alexeev, D. G.; Lipanov, A. A.; Skuratovskii, I. Y. Nature 1987, 325, 821–823.
33. Albiser, G.; Premilat, S. CR Acad Sci III 1997, 320, 735–739.
34. Letellier, R.; Ghomi, M.; Taillandier, E. J Biomol Struct Dynam 1987, 4 , 663–683.
35. Zuo, E. T.; Tanious, F. A.; Wilson, D.; Zon, G.; Tan, G.-S.; Wartell, R. M. Biochemistry 1990, 29, 4446–4456.
36. Buckin, V. A.; Kankiya, B. I.; Bulichov, N. V.; Lebedev, A. V.; Gukovsky, I. Y.; Chuprina, V. P.; Sarvazyan, A. P.; Williams, A. R. Nature 1989, 340, 321–322.
37. Ganunis, R. M.; Guo, H.; Tullius, T. D. Biochemistry 1996, 35, 13729–13732.
38. Thomas, G. J., Jr. Annu Rev Biophys Biomol Struct 1999, 28, 1–27.
39. Thomas, G. J., Jr.; Tsuboi, M. Adv Biophys Chem 1993, 3, 1–70.
40. Thomas, G. J., Jr.; Wang, A. H.-J. Nucleic Acids Mol Biol 1988, 2, 1–30.
41. Prescott, B.; Steinmetz, W.; Thomas, G. J., Jr. Biopolymers 1984, 23, 235–256.
42. Yoon, C.; Prive, G. G.; Goodsell, D. S.; Dickerson, R. E. Proc Natl Acad Sci USA 1988, 85, 6332–6336.
43. Benevides, J. M.; Stow, P. L.; Ilag, L.; Incardona, N. L.; Thomas, G. J., Jr. Biochemistry 1991, 30, 4855–4863.
44. Toyama, A.; Takino, Y.; Takeuchi, H.; Harada, I. J Am Chem Soc 1993, 115, 11092–11098.
45. Terpstra, P. A.; Otto, C.; Greve, J. J Chem Phys 1997, 106, 846–848.
46. Aida, M.; Kaneko, M.; Dupuis, M.; Ueda, T.; Ushizawa, K.; Ito, G.; Kumakura, A.; Tsuboi, M. Spectrochim Acta 1997, 53A, 393–407.
47. Lord, R. C.; Thomas, G. J., Jr. Spectrochim Acta 1967, 23A, 2551–2591.
48. Fujimoto, N.; Toyama, A.; Takeuchi, H. J Mol Struct 1998, 447, 61–69.

49. Puhl, H. L.; Behe, M. J. J Mol Biol 1995, 245, 559–567.

50. Scheffler, I. E.; Elson, E. L.; Baldwin, R. L. J Mol Biol 1968, 36, 291–304.

51. Scheffler, I. E.; Elson, E. L.; Baldwin, R. L. J Mol Biol 1970, 48, 145–171.

52. Westhof, E. Annu Rev Biophys Biophys Chem 1988, 17, 125–144.

53. Falk, M.l Hartman, K. A.; Lord, R. C. J Am Chem Soc 1963, 85, 391–394.

54. Feig, M.; Pettitt, B. M. Biopolymers 1998, 48, 199–209.

55. Kopka, M. L.; Fratini, A. V.; Drew, H. R.; Dickerson, R. E. J Mol Biol 1983, 163, 129–146.

56. Chuprina, V. P. FEBS Lett 1985, 186, 98–102.

57. Chuprina, V. P. Nucleic Acids Res 1987, 15, 293–311.

58. Shui, X.; McFail-Isom, L.; Hu, G. G.; Williams, L. D. Biochemistry 1998, 37, 8341–8355.

59. Chiu, T. K.; Kaczor-Grzeskowiak, M.; Dickerson, R. E. J Mol Biol, 1999, 292, 589–608.

60. Radhakrishnan, I.; Patel, D. J. Structure 1994, 2, 395–405.

61. Liepinsh, E.; Otting, G.; Wuthrich, K. Nucleic Acids Res 1992, 20, 6549–6553.

62. Denisov, V. P.; Carlstrom, G.; Venu, K.; Halle, B. J Mol Biol 1997, 268, 118–136.

63. Halle, B.; Denisov, V. P. Biopolymers 1998, 48, 210–233.

64. Spink, C. H.; Chaires, J. B. Biochemistry 1999, 38, 496–508.

65. Schneider, B.; Berman, H. M. Biophys J 1995, 69, 2661–2669.

66. Jóhannesson, H.; Halle, B. J Am Chem Soc 1998, 120, 6859–6870.

67. Chalikian, T. V.; Breslauer, K. J. Biopolymers 1998, 48, 264–280.